Environ Sci Pollut Res (2016) 23:18609–18620
DOI 10.1007/s11356-016-7061-y

RESEARCH ARTICLE

Highly selective catalytic reduction of NO via SO_2/H_2O-tolerant spinel catalysts at low temperature

Xuanxuan Cai[1] · Wei Sun[1] · Chaochao Xu[1] · Limei Cao[1] · Ji Yang[1]

Received: 12 March 2016 / Accepted: 8 June 2016 / Published online: 15 June 2016

Abstract Selective catalytic reduction of NO_X by hydrogen (H_2-SCR) in the presence of oxygen has been investigated over the $NiCo_2O_4$ and Pd-doped $NiCo_2O_4$ catalysts under varying conditions. The catalysts were prepared by a sol-gel method in the presence of oxygen within 50–350 °C and were characterized using XRD, BET, EDS, XPS, Raman, H_2-TPR, and NH_3-TPD analysis. The results demonstrated that the doped Pd could improve the catalyst reducibility and change the surface acidity and redox properties, resulting in a higher catalytic performance. The performance of $NiCo_{1.95}Pd_{0.05}O_4$ was consistently better than that of $NiCo_2O_4$ within the 150–350 °C range at a gas hourly space velocity (GHSV) of 4800 mL g^{-1} h^{-1}, with a feed stream containing 1070 ppm NO, 10,700 ppm H_2, 2 % O_2, and N_2 as balance gas. The effects of GHSV, NO/H_2 ratios, and O_2 feed concentration on the NO conversion over the $NiCo_2O_4$ and $NiCo_{1.95}Pd_{0.05}O_4$ catalysts were also investigated. The two samples similarly showed that an increase in GHSV from 4800 to 9600 mL h^{-1} g^{-1}, the NO/H_2 ratio from 1:10 to 1:1, and the O_2 content from 0 to 6 % would result in a decrease in NO conversion. In addition, 2 %, 5 %, and 8 % H_2O into the feed gas had a slightly negative influence on SCR activity over the two catalysts. The effect of SO_2 on the SCR activity indicated that the $NiCo_{1.95}Pd_{0.05}O_4$ possesses better SO_2 tolerance than $NiCo_2O_4$ catalyst does.

Keywords SCR · NO_X · Hydrogen · Flue gas · Gas treatment · SO_2/H_2O-tolerant

Responsible editor: Bingcai Pan

Highlights The Pd-doped nickel cobaltate spinels achieved 95 % NO conversion with N_2 selectivity of 100 % in the 200~250 °C range.
SCR of NO_X by hydrogen in the presence of oxygen has been significantly improved via doping Pd into $NiCo_2O_4$.
The prepared $NiCo_{1.95}Pd_{0.05}O_4$ catalyst possessed better H_2O and SO_2 tolerance than $NiCo_2O_4$.

✉ Ji Yang
yangji@ecust.edu.cn

[1] School of Resources and Environmental Engineering, State Environmental Protection Key Laboratory of Environmental Risk Assessment and Control on Chemical Process, East China University of Science and Technology, Shanghai 200237, People's Republic of China

Introduction

Nitrogen oxides (NO_X), including NO, NO_2, N_2O, N_2O_3, N_2O_4, and N_2O_5, are mainly derived from fossil fuel combustion (Costa and Efstathiou 2007b). NO_X are the major air pollutants that are greatly hazardous to human health and the environment (Xiaoling et al. 2012), causing negative effects such as photochemical smog, acid rain, ozone depletion, ground-level ozone, and greenhouse effects (Qi et al. 2006). A number of techniques have been developed to reduce the emission of NO_X. Among them, the selective catalytic reduction of NO_X by ammonia (NH_3-SCR) is a well-known and widely industrialized NO_X control technology for stationary sources such as power plants and nitric acid plants (Li et al. 2010b). Generally, V_2O_5-WO_3 (MO_3)/TiO_2 is employed as NH_3-SCR catalysts (Grossale et al. 2008). However, many problems are encountered in the use of NH_3-SCR technology, namely catalyst deterioration, NH_3 slip (emissions of unreacted toxic ammonia), ash odor, air heater fouling, and a high running cost (Olympiou and Efstathiou 2011).

H_2-SCR has many advantages; for instance, hydrogen as a reductant does not induce any second pollutants and has high activity to reduce NO_X efficiently at the lowest possible

temperature (Kim and Hong 2010; Machida et al. 2001). Especially for industrial sites where H_2 is readily available, H_2-SCR is regarded as a possible alternative for NH_3-SCR. The catalyst is the most central technology in any H_2-SCR process, and its performance directly affects the removal of nitrogen oxides (Koebel et al. 2001; Weirong et al. 2012). Currently, the catalysts of H_2-SCR primarily contain supported noble metal oxides (Jun Yub et al. 2003; Yang and Jung 2009), among which the Pt-based and Pd-based catalysts have been revealed to possess good catalytic activity at relatively low temperatures (Chiarello et al. 2007; Costa and Efstathiou 2007a; Qing et al. 2010; Schott et al. 2009). For example, Costa and Efstathiou (2007a) had reported that the Pt/MgO-CeO_2 catalyst exhibited a maximum of 95 % NO conversion and 78~92 % N_2 selectivity within the 100–400 °C range. Higher than 90 % NO_X conversion within 170–300 °C was presented in the Pd/SiO_2 catalyst (Qing et al. 2010). Chiarello et al. (2007) investigated the catalytic reduction of NO_X by H_2 over Pd-based catalysts with a support consisting of $LaCoO_3$. The 0.5 wt% Pd/$LaCoO_3$ catalyst exhibited a maximum of approximately 100 % NO conversion and over 78 % N_2 selectivity at 150 °C.

Nevertheless, noble metals are rare and expensive and they are sensitive to sulfur poisoning. These factors limit their large-scale applications. Therefore, new highly efficient catalysts need to be searched to replace Pt-based and Pd-based catalysts for H_2-SCR for NO_X. Due to their low price, ready synthesis, and good redox property, transition metal oxides have been widely used as catalysts in various reactions (Auxilia et al. 2014; Chiu et al. 2015). Among them, spinel-type oxides have been widely studied because of their unique structure characteristics, and these oxide catalysts can simultaneously reduce NO_X and soot at comparatively low temperatures (possibly within the range typical of diesel exhaust 150–380 °C) (Fino et al. 2008). Chen et al. (2009) had reported that the CuCoOx/TiO_2 catalyst exhibited a maximum of 98.9 % NO conversion at 200 °C. Du et al. (2014) had reported that Co_3O_4 showed high performance on the removal of low-concentration (10 ppm) NO at room temperature.

Nickel cobaltite ($NiCo_2O_4$) is a mixed-metal oxide spinel that possesses interesting magnetic properties, rich redox chemistry, good electronic conductivity, and high electrochemical activity (Kim et al. 2000; Rui et al. 2013). In the recent research, $NiCo_2O_4$ is usually explored as an electrode material (Chi et al. 2006; Xu et al. 2014) and has rare reports about the catalytic reduction performance in the SCR reaction. Wang et al. (2015b) had reported that $NiCo_2O_4$ possessed the highest catalytic activity within 50–400 °C, with NO_X conversion of more than 70 % at 150 °C and N_2 selectivity of more than 90 % at 100–400 °C. Therefore, we choose nickel cobaltite as a model catalyst.

Generally, doped noble metal can improve the catalytic activity and reduce the operating temperature. Palladium is less expensive and more abundant than platinum (Gaspar and Dieguez 2000), and Pd as an active component shows high activity for H_2-SCR and is highly active for H_2 activation (Li et al. 2012). The exceptional performance is due to the high dispersion of Pd in the catalyst that forms the Pd-NO intermediates, which adsorb more NO on the catalyst surface and are reduce to N_2 by hydrogen with high N_2 selectivity (Li et al. 2008). Rodríguez and Saruhan (2010) reported that the highly active centers could be formed by the interaction sites between Pd and supports and high NO_X conversion and N_2 selectivities could be achieved by the synergistic effects of palladium and perovskites. Moreover, the synergistic effects efficiently enhance H_2 temperature-programmed reduction (H_2-TPR). Besides, Xu et al. (2015) had researched that doped Pd could make $NiFe_{1.95}Pd_{0.05}O_4$ increase acidity, reducibility, and catalytic activity.

NO was selected as a model nitrogen oxide in the simulated gas (Wang et al. 2009), because nitrogen monoxide accounts for 95–99 % of all nitrogen oxide emissions in flue gas (Fritz and Pitchon 1997). And the Pd-doped nickel cobaltite catalyst was successfully prepared through a sol-gel auto-ignition method and exhibited good catalytic performance for the selective catalytic reduction of NO by H_2 in the presence of oxygen at a low temperature. And we have considered the effects of the gas hourly space velocity (GHSV), NO/H_2 ratios, and O_2 feed concentration on the SCR activity. For practical consideration, we also investigated the durability of the catalyst and its tolerance to SO_2 and H_2O, respectively.

Materials and methods

Catalyst preparation

The catalyst used in this research was prepared via a sol-gel method using inorganic salts. All of the chemicals were of analytical grade and used without further purification. The compounds were weighed by analytical balance with the molar ratio of citric acid/$Ni(NO_3)_3{\cdot}6H_2O$/$Co(NO_3)_3{\cdot}6H_2O$/$PdCl_2$ = 3:1:1.95:0.05. Then, these compounds were dissolved in 50 mL deionized water with a concentration of 0.1 mol nitrate precursor (Jauhar et al. 2013). The pH of the mixture solution was additionally adjusted to 5–6 by slowly adding the ammonia solution, then the resulting solution was mixed together under stirring at room temperature for 3 h, and the sol was heated at 80 °C to form a wet gel; afterwards, the gel was dried at 130 °C. After drying, the obtained material was ground into fine powder. In order to obtain crystallized $NiCo_{1.95}Pd_{0.05}O_4$, the powder was calcinated in Muffle furnace at 400 °C for 4 h. Spinel $NiCo_2O_4$ was prepared in similar way with the only difference that merely the molar ratio of citric acid/$Ni(NO_3)_3{\cdot}6H_2O$/$Co(NO_3)_3{\cdot}6H_2O$/$PdCl_2$ was 3:1:2.

According to the drying and roasting process, the particles were easy to reunite and affect the catalyst activity, so about 5 mL polyethylene glycol (PEG) 400 was added to ensure high specific surface area and uniform particle size (Fan and Huang 2011).

Catalyst characterization

The as-prepared products were characterized by powder X-ray diffraction (XRD) using a Rigaku D/Max 2550 diffractometer (Japan) with Cu Kα radiation (λ = 1.54056 Å) operating at 40 kV and 100 mA. The elemental composition of the samples was characterized by energy-dispersive spectrometer (EDS) using a Falion 60s spectrometer. The Brunauer–Emmett–Teller (BET) surface area, average particle size, and pore size of the catalysts were measured with a nitrogen adsorption instrument (Micromeritics, TriStar II 3020) using N_2 gas as an adsorbent at the temperature of liquid nitrogen. Prior to BET analysis, the samples were degassed at 300 °C for 3 h.

The X-ray photoelectron spectroscopy (XPS) analysis was conducted in a Quantum 2000 Scanning ESCA Microprobe (Physical Electronics). The instrument uses a focused monochromatic Al Kα X-ray (1486.7 eV) source operated at a 100 W and 100-μm-diameter beam. The binding energy scale was calibrated using the carbon C1s at 284.6 eV for known standards. The de-convolution of XPS peak was performed with the CasaXPS program. The Raman spectroscopy experiments were carried out on an Iuvia microscope instrument (Iuvia Reflerx) with a wavelength of 514.5 nm.

H_2-TPR and temperature-programmed desorption of ammonia (NH_3-TPD) were performed on AutoChem II 2920 equipped with a thermal conductivity detector (TCD) detector. Prior to the H_2-TPR or NH_3-TPD analysis, 50 mg of the oven-dried sample was pretreated in a He stream at 300 °C for 60 min to remove the adsorbed H_2O and other gases followed by cooling to room temperature. After that, the H_2-TPR analysis was performed using a 10 % H_2/Ar mixture at a flow rate of 40 mL/min with a heating rate of 10 °C/min to 800 °C, while the NH_3-TPD analysis was carried out by 10 % NH_3/He mixture with a total flow rate of 40 mL/min at 50 °C for 60 min. After NH_3 adsorption, the sample was purged by He (40 mL/min) for another 60 min. The desorption profile was recorded using a TCD by heating the sample to 600 °C at 10 °C/min under a flow of He (50 mL/min).

Catalyst activity testing

The selective catalytic reduction of NO by hydrogen was carried out in a fixed-bed flow micro-reactor, the catalyst bed temperature was controlled by thermocouple which was interpolated into the fixed-bed reactor, and reactor was heated through an Al-518/518P-type artificial intelligence temperature controller. A sample weighed 1 g, and the reactant gas composites consisted of 1071 ppm NO; 1071–10,710 ppm H_2 (the concentration was based on the ratio of NO to H_2); 0–6 % O_2; 2 %, 5 %, and 8 % H_2O (when used); 100, 300, and 500 ppm SO_2 (when used); and the balance N_2. These gases were fed from compressed cylinders provided by Jia Jie Specialty Gases (Shanghai, China) and adjusted with Brooks thermal mass flow controllers. The catalyst was fixed by silica pellets and quartz wool and placed in the constant temperature zone of the tubular reactor. The total flow of the inlet gas and the gas hourly space velocity were based on the change of gas conditions. The gas effluent stream from the reactor was analyzed by a Chemiluminescent NO–NO_2–NO_X Analyzer (Thermo Scientific, model 42i), and the nitric oxide conversion was indicated using the following equation:

$$X_{\mathrm{NO}}(\%) = \frac{[\mathrm{NO}]_{\mathrm{inlet}} - [\mathrm{NO}]_{\mathrm{outlet}}}{[\mathrm{NO}]_{\mathrm{inlet}}} \times 100\% \quad (1)$$

Among them, X_{NO} represents the NO conversion and $[\mathrm{NO}]_{\mathrm{inlet}}$ and $[\mathrm{NO}]_{\mathrm{outlet}}$ show the inlet and outlet concentrations of NO in the gas mixture at steady state, respectively.

The Thermo Scientific NO–NO_2–NO_X Analyzer revealed that the NO_X was the sum of NO, NO_2, and less low-state nitrogen oxides, and the X_{NO_X} represented the total NO_X conversion rate.

$$X_{\mathrm{NO}_X}(\%) = \frac{[\mathrm{NO}_X]_{\mathrm{inlet}} - [\mathrm{NO}_X]_{\mathrm{outlet}}}{[\mathrm{NO}_X]_{\mathrm{inlet}}} \times 100\% \quad (2)$$

where the $[\mathrm{NO}_X]_{\mathrm{inlet}}$ and $[\mathrm{NO}_X]_{\mathrm{outlet}}$ show the inlet and outlet concentrations of NO in the gas mixture at steady state, respectively. The N_2 selectivity was calculated as follows:

$$S_{\mathrm{N}_2}(\%) = \frac{X_{\mathrm{NO}_X} \cdot [\mathrm{NO}]_{\mathrm{inlet}}}{X_{\mathrm{NO}} \cdot [\mathrm{NO}]_{\mathrm{inlet}}} \times 100\% \quad (3)$$

In this equation, the $X_{\mathrm{NO}} \cdot [\mathrm{NO}]_{\mathrm{inlet}}$ expresses the amount of nitric oxide in the transformation, while the $X_{\mathrm{NO}_X} \cdot [\mathrm{NO}]_{\mathrm{inlet}}$ expresses the amount of nitrogen from the transformation of nitric oxide.

Results and discussion

Catalyst characterization

Structural and textural properties

The XRD patterns of the samples used in this study are shown in Fig. 1a. The major peaks of the samples at ca. 2θ = 18.9°, 31.1°, 36.7°, 38.4°, 44.6°, 55.4°, 59.1°, and 65.1° could be indexed to (111), (220), (311), (222), (400), (422), (511), and (440) crystal planes of spinel $NiCo_2O_4$, respectively. It could be seen that the samples were a spinel cubic structure which

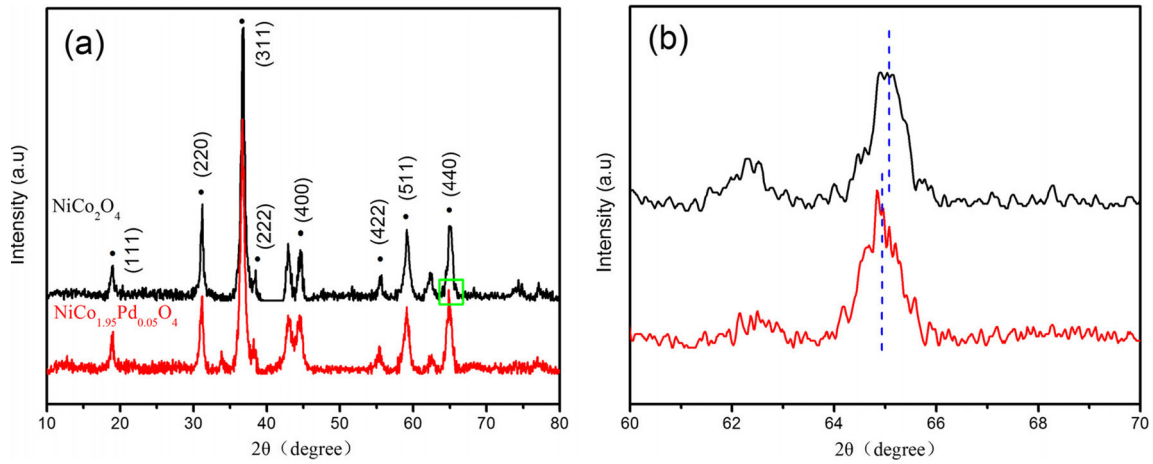

Fig. 1 **a** XRD patterns of $NiCo_2O_4$ and $NiCo_{1.95}Pd_{0.05}O_4$ used in this study. **b** XRD peak positions of (440) crystal planes

were in good agreement with the standard pattern (JCPDS No. 73-1702) (Xu et al. 2014). While the XRD pattern of $NiCo_{1.95}Pd_{0.05}O_4$ was similar to that of $NiCo_2O_4$, the diffraction angle theta of (440) crystal planes slightly shifted from 65.1° to 64.9°, which is shown in Fig. 1b. These results indicated that the heavier and larger Pd^{2+} ions substituted the Co^{2+} ions in the structure of the nickel cobaltite spinel, resulting in a small angle deviation of XRD peaks (Kavas et al. 2009). And the Pd doping did not cause a significant change in the crystallinity of the samples, possibly due to the palladium that replaced Co without distorting the spinel structure; therefore, the $NiCo_{1.95}Pd_{0.05}O_4$ sample also maintained the spinel cubic structure.

The average crystalline size of $NiCo_2O_4$ and $NiCo_{1.95}Pd_{0.05}O_4$ was estimated to be 32.2 and 26.7 nm using Scherrer's formula based on the (422) peak, respectively (Lou et al. 2008). Scherrer's formula is as follows:

$$D = \frac{K\lambda}{\beta\cos\theta} \tag{4}$$

Among which, D is crystalline size, K is constant, λ is X-ray wavelength (0.154056 nm), β is peak half-high width, and θ is the diffraction angle theta. Due to nickel cobaltite's spinel cubic structure, K should be changed to 0.943 and a half-high width should be converted into a radian system, $[(\beta / 180) \times 3.14]$.

BET and EDS analysis

The BET surface areas, average particle size, and pore size of the studied $NiCo_2O_4$ and $NiCo_{1.95}Pd_{0.05}O_4$ were summarized in Table 1. The surface areas of the $NiCo_2O_4$ and $NiCo_{1.95}Pd_{0.05}O_4$ samples were 14.9956 and 12.6566 $m^2\ g^{-1}$, respectively, while the average particle sizes were 14.0774 and 15.4802 nm, respectively, which had the reverse order compared to the surface area values. Generally, the larger the particle size, the smaller the BET area. The elemental composition of the samples was investigated using an EDS, as shown in Table 1. The Co/Ni atomic ratio (we chose Ni for comparison due to the stoichiometric amount being 1 in all of the studied samples) for $NiCo_2O_4$ was 2.03, which was consistent with the stoichiometric ratio. Due to the palladium doping, the Co/Ni atomic ratio of $NiCo_{1.95}Pd_{0.05}O_4$ was 1.92, deviating slightly from the theoretical ratio of 1.95. The Pd/Ni atomic ratio was 0.049, which was consistent with the theoretical value of 0.05.

H_2-TPR and NH_3-TPD analysis

In order to investigate the reducibility and acidic properties of the $NiCo_2O_4$ and $NiCo_{1.95}Pd_{0.05}O_4$, the as-prepared samples were characterized by H_2 temperature-programmed reduction (H_2-TPR) and temperature-programmed desorption of ammonia (NH_3-TPD) analysis, respectively. As shown in Fig. 2a, there were three distinct reduction peaks in $NiCo_2O_4$, and the peaks appeared at 253 and 360 °C, corresponding to the reduction steps of Co^{3+} to Co^{2+} and Co^{2+} to Co^0, respectively (Gou et al. 2013; Lim et al. 2015), while the peak appeared at 315 °C, which was attributed to the reduction of Ni^{2+} to Ni^0. However, in comparison to $NiCo_2O_4$, the H_2-TPR profile of the $NiCo_{1.95}Pd_{0.05}O_4$ catalyst showed one slight peak and one strong broad peak. The slight peak at 129 °C was assigned to the reduction of Pd^{2+} to Pd^0 (Giraudon et al. 2007; Ling et al. 2015), which was observed in pure Ni-Co spinel. And the strong broad peak within the range of 200–350 °C was formed by three reduction peaks fully overlapped, which corresponded to the reductions of Co^{3+} to Co^{2+} at 223 °C, Ni^{2+} to Ni^0 at 286 °C, and Co^{2+} to Co^0 at 316 °C. Compared to $NiCo_2O_4$, the reduction peaks of $NiCo_{1.95}Pd_{0.05}O_4$ shifted to low temperature, which indicated that the H_2 consumption was raised, enhancing the redox properties of catalysts. In addition, the TPR peak areas were an indicator to determine the reducibility of catalyst; the greater the peak area, the stronger the reducibility. The peak areas

Table 1 Physical and chemical properties of the studied catalysts

Catalysts	S_{BET} ($m^2\ g^{-1}$)	$D_{particle}$ (nm)	D_{pore} (nm)	Elemental composition (at.%)				
				Ni	Co	Pd	Pd/Ni	Co/Ni
$NiCo_2O_4$	14.9956	400.1164	14.0774	18.78	38.26	0.00	0.000	2.037
$NiCo_{1.95}Pd_{0.05}O_4$	12.6566	474.0594	15.4802	20.29	38.97	1.00	0.0493	1.921

of H_2-TPR were provided in Table 2. It could be seen that the Pd-containing nickel cobaltate exhibited relatively higher TPR areas than $NiCo_2O_4$, indicating that the palladium doping could improve the catalyst reducibility.

The acidic properties of the as-prepared samples were shown in Fig. 2b. The NH_3 adsorbed on the acid sites and then desorbed at different temperature regions, which was determined by the strength of acid sites and the amount of acid, respectively. The NH_3 desorption below 400 °C corresponded to the weak- and medium-strength acid sites (Imran et al. 2013). Nevertheless, the TPD profile of $NiCo_2O_4$ showed a broad NH_3 desorption peak from 100 to 350 °C, which was assigned to the NH_3 desorbed by weak- and medium-strength acid sites. Moreover, the acid amount could be determined by the TPD peak areas and the size of peak area corresponded to the amount of acid. Table 2 showed the NH_3-TPD peak areas. Compared to $NiCo_2O_4$, $NiCo_{1.95}Pd_{0.05}O_4$ slightly increased the peak areas from 100 to 350 °C, indicating that $NiCo_{1.95}Pd_{0.05}O_4$ showed a relatively more acidic amount than $NiCo_2O_4$.

Raman analysis

$NiCo_2O_4$ is an inverse spinel with tetragonal (A site) positions occupied by mostly Co^{3+} and octahedral (B site) positions occupied by nearly equal concentrations of Ni^{2+} and Co^{3+} (Iliev et al. 2013). In order to further understand the composition and structural features of the $NiCo_2O_4$ and $NiCo_{1.95}Pd_{0.05}O_4$, the samples were characterized with Raman spectroscopy. The typical Raman spectrum was shown in Fig. 3; the peaks of $NiCo_2O_4$ at 183, 465, 509, and 651 cm^{-1} corresponded to F_{2g}, E_{1g}, F_{2g}, and A_{1g} models of $NiCo_2O_4$, respectively, and the Co–O and Ni–O stretching vibrations could be detected in the Raman spectrum. These results were well consistent with previously reported literatures (Babu et al. 2014; Li et al. 2015; Liu et al. 2013). Moreover, the peaks at 181, 418, 501, and 644 cm^{-1} corresponded to F_{2g}, E_{1g}, F_{2g}, and A_{1g} models of $NiCo_{1.95}Pd_{0.05}O_4$, respectively. Compared with that of $NiCo_2O_4$, the Raman spectra of the Pd-substituted nickel cobaltate ($NiCo_{1.95}Pd_{0.05}O_4$) exhibited a shift toward lower wave number, which was the result of the heavier and larger Pd^{2+} ions substituting the Co^{2+} ions in the structure of the nickel cobaltite spinel.

XPS analysis

In order to investigate the chemical bonding states and compositions of surface elements of as-synthesized $NiCo_2O_4$ and $NiCo_{1.95}Pd_{0.05}O_4$, the samples were studied by X-ray photoelectron spectroscopy (XPS), and the results were shown in Fig. 4a–d. The Ni, Co, O, and Pd elements were detected for the prepared samples.

The high-resolution spectrum for the O1s region in Fig. 4a showed two peaks at binding energies of around 529.1 and 530.8 eV, respectively, which had been denoted as O1

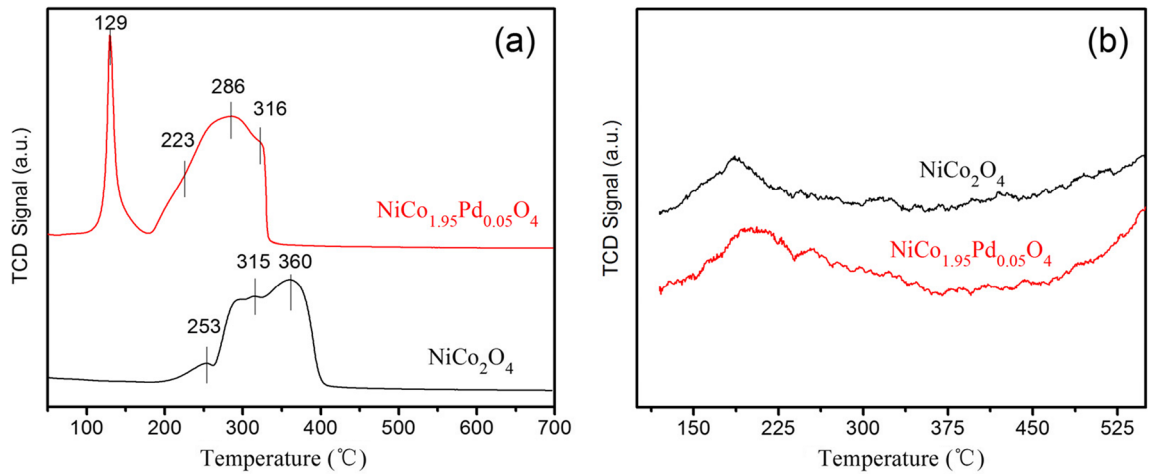

Fig. 2 H_2-TPR and NH_3-TPD profiles of $NiCo_2O_4$ and $NiCo_{1.95}Pd_{0.05}O_4$ used in this study. **a** H_2-TPR. **b** NH_3-TPD

Table 2 The peak areas of H_2-TPR and NH_3-TPD

Catalysts	H_2-TPR								Total	NH_3-TPD	
	Peak 1		Peak 2		Peak 3		Peak 4			Peak	
	T (°C)	Area	*T* (°C)	Area	*T* (°C)	Area	*T* (°C)	Area		*T* (°C)	Area
$NiCo_2O_4$	253	3.1764	315	11.5537	360	17.7736	0	0.0000	32.5037	186	0.2000
$NiCo_{1.95}Pd_{0.05}O_4$	129	11.1585	223	4.3780	286	26.4388	316	3.5521	45.5274	206	0.3189

The unit of the peak area was defined as 1. The dosage of the samples was the same in the measurement of H_2-TPR and NH_3-TPD

(529.1 eV) and O2 (530.8 eV). The O1 at the low energy of 529.1 eV was typical of the O atoms in the O–Co/Ni bonding. And the O_2 at 530.8 eV was a characteristic of the as-prepared $NiCo_2O_4$ samples, which corresponded to a number of defect sites with low-oxygen coordination in the material with small particle size (Kim et al. 2000; Liu et al. 2013; Rui et al. 2013). The Co2p binding energies and peak shape were similar for the two preparations (Fig. 4b) and yield binding energies of 779.8 and 794.7 eV for the 2p3/2 and 2p1/2 transitions, respectively (Kim et al. 2000). XPS spectra of Co2p3/2 in the two preparations showed two main peaks of binding energies at 779.4 and 781.4 eV, which were assigned to the surface Co^{3+} and Co^{2+} species, respectively (Wang et al. 2015b). And this indicated that there were only a few Co^{2+} species in the octahedral sites and most of the low-spin Co^{3+} species occupied the octahedral sites (Babu et al. 2014; Kim et al. 2000).

The Ni2p spectra given in Fig. 4c were fitted considering two spin-orbit doublets as a characteristic of Ni^{2+} and Ni^{3+} and two shake-up satellites. The fitting peaks at the binding energy of 854.4 and 871.6 eV were indexed to Ni^{2+}, while the fitting peaks at the binding energy of 856.43 and 873.8 eV were ascribed to Ni^{3+}, respectively (Li et al. 2015, 2010a; Yu et al. 2016). The Pd3d spectra, as presented in Fig. 4d, showed two peaks at the binding energy of 337.1 eV for 3d5/2 and 342.5 eV for 3d3/2, respectively. The Pd5/2 binding energy was closed to the value of 336.9 which is a characteristic of Pd^{2+}, indicating that the Pd doped in the as-prepared $NiCo_{1.95}Pd_{0.05}O_4$ sample (Giraudon et al. 2007; Hu et al. 2011; Ling et al. 2015).

These results exhibited that the surface of the as-synthesized $NiCo_2O_4$ that contained Ni^{2+}, Ni^{3+}, Co^{2+}, and Co^{3+} (Moni et al. 2014), while the $NiCo_{1.95}Pd_{0.05}O_4$ also contained Pd^{2+} except the common elements.

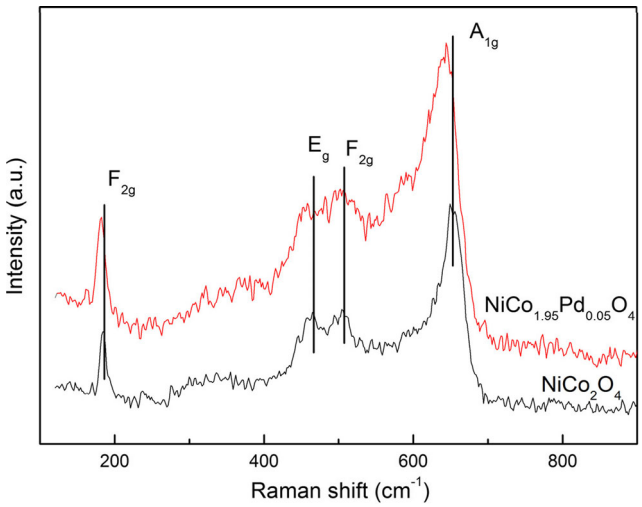

Fig. 3 Raman profiles of $NiCo_2O_4$ and $NiCo_{1.95}Pd_{0.05}O_4$ used in this study

Catalyst performance

SCR activity of the $NiCo_2O_4$ and $NiCo_{1.95}Pd_{0.05}O_4$ catalysts

Figure 5 shows the results of the NO conversion and N_2 selectivity over the $NiCo_2O_4$ and $NiCo_{1.95}Pd_{0.05}O_4$ in the temperature range of 50–350 °C with a GHSV of 4800 mL g^{-1} h^{-1} in the presence of 2 % O_2. As shown in Fig. 5a, as the reaction temperature increased, the NO conversion firstly increased then decreased over the $NiCo_{1.95}Pd_{0.05}O_4$ catalyst. While the SCR activity over the $NiCo_2O_4$ catalyst was always increasing until it reached the maximum NO conversion. The highest NO conversion of the $NiCo_2O_4$ catalyst was approximately 40.05 % at 350 °C; yet, the N_2 selectivity over the $NiCo_2O_4$ catalyst was only 60~80 %, which is illustrated in Fig. 5b. The NO conversion over the $NiCo_{1.95}Pd_{0.05}O_4$ catalyst was higher than 90 % at a suitable temperature of 200–250 °C with the maximum of 94.65 % at 230 °C. And the N_2 selectivity was higher than 90 % in the whole 130–350 °C range, with the maximum closed to 100 % at the 200–270 °C range.

Moreover, a previous study showed that the content of O_2 was a crucial parameter for the H_2-SCR reaction (Yang et al. 2011; Yuan et al. 2013). The combustion of fuel was not sufficient in the old burners, which resulted in the high oxygen content of 6~12 %. However, the new type of circulating fluidized bed burns the fuel more efficiently, resulting in the low oxygen content of 4~6 % (Huilin et al. 2000). Hence, in our study, the highest oxygen content was chosen to be 6 %. In general, oxygen can inhibit NO removal efficiency by oxidizing H_2 to H_2O, but it also oxidizes NO into adsorbed nitrite/nitrate on the surface to enhance the reduction reaction by hydrogen in the H_2-SCR process (Machida et al. 2001; Wei

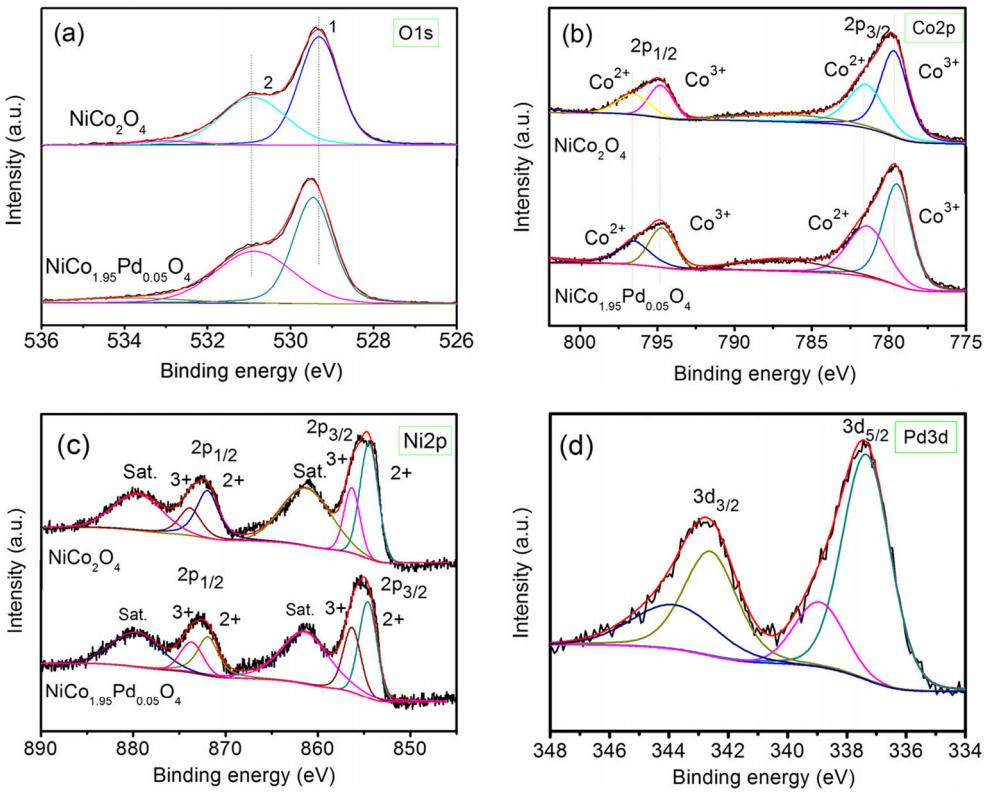

Fig. 4 XPS spectra of $NiCo_2O_4$ and $NiCo_{1.95}Pd_{0.05}O_4$ used in this study. **a** O1s. **b** Co2p. **c** Ni2p. **d** Pd3d

et al. 2012). Hence, the effect of the oxygen concentration ($[O_2]$ = 0 %, 2 %, 4 %, and 6 %) in the feed gas over the $NiCo_{1.95}Pd_{0.05}O_4$ and $NiCo_2O_4$ catalysts was investigated, which also consisted of 1070 ppm NO/10,700 ppm H_2/*x* % O_2/N_2 at a temperature range of 50–350 °C with a GHSV of 4800 mL g^{-1} h^{-1}.

The oxygen content in the flue gas from the circulating fluidized bed boiler is generally 4~6 % (Huilin et al. 2000). Therefore, experiments were performed to examine the O_2 tolerance of the prepared catalysts. As illustrated in Fig. 5c, under O_2-free reaction conditions, a higher removal efficiency of NO was achieved and an efficiency of 100 % over the $NiCo_2O_4$ catalysts was stabilized within a temperature range of 250–350 °C. As the O_2 content increased from 0 % to 6 %, the deNO_X performance rapidly decreased and the maximum NO conversion decreased from 100 to 30.77 % at the 350 °C. As shown in Fig. 5d, the high NO conversion of 100 % over $NiCo_{1.95}Pd_{0.05}O_4$ was stabilized within a wider temperature range of 150–350 °C in the absence of oxygen, indicating that the doped Pd improved the catalytic activity and shifted the reaction temperature of the efficiency of 100 % from 250 to 150 °C. When the O_2 increased to 2 %, the maximum NO conversion over $NiCo_{1.95}Pd_{0.05}O_4$ only changed to 94 % at the 230 °C; as the O_2 content increased, the SCR still exhibited good activity for NO reduction, with the maximum NO conversion of 81.16 % with 4 % O_2 at 230 °C and 61 % in the presence of 6 % O_2 at 230 °C, proving that Pd incorporation not only significantly improves the catalytic activity but also increases the O_2 tolerance ability (Wei et al. 2012).

To sum up, the $NiCo_{1.95}Pd_{0.05}O_4$ catalyst showed higher catalytic performance as well as greatly reduced the reaction temperature of the maximum removal efficiency. Hence, the $NiCo_{1.95}Pd_{0.05}O_4$ catalyst was suitable for the selective catalytic reduction of NO by H_2 in the presence of oxygen at a low temperature. Therefore, Pd played a very important role in the nickel cobaltite catalyst in the H_2-SCR reaction. In addition, palladium did not destroy the spinel structure of $NiCo_2O_4$ when it doped in nickel cobaltite, which was consistent with the XRD results. And from the H_2-TPR and NH_3-TPD activity tests, the $NiCo_{1.95}Pd_{0.05}O_4$ exhibited relatively high TPR areas, reduction level, and slightly larger acidity than $NiCo_2O_4$. All these factors resulted in the better catalytic performance of $NiCo_{1.95}Pd_{0.05}O_4$.

Effect of GHSV and NO/H_2 ratio

In general, GHSV could significantly affect the NO conversion rate at low temperature, and it was believed that it has less effect on the conversion rate at high temperature (Qi et al. 2006). Consequently, the H_2-SCR activity of the $NiCo_2O_4$ and $NiCo_{1.95}Pd_{0.05}O_4$ catalysts at different GHSVs (from 4800 to 9300 mL h^{-1} g^{-1}) and NO and H_2 feed concentration ratios (NO/H_2 = 1:10–1:1) were investigated at a temperature

range of 50–350 °C in the presence of 2 % O_2, and the results are shown in Fig. 6.

As shown in Fig. 6a, the NO conversion over the $NiCo_2O_4$ catalyst decreased with the increasing GHSV. When the GHSV was 4800 mL h^{-1} g^{-1}, the maximum NO conversion was up to 40.5 % at 350 °C, while when the GHSV increased to 6960 and 9300 mL h^{-1} g^{-1}, the maximum conversion decreased to 35 % and 31 %, respectively. However, in contrast with $NiCo_2O_4$, the NO conversion faintly decreased over the $NiCo_{1.95}Pd_{0.05}O_4$ catalyst with the increase of the GHSV from 4800 to 9600 mL h^{-1} g^{-1} at the reaction temperature of 125–350 °C, which was shown in Fig. 6b. When the GHSV was 4800 mL h^{-1} g^{-1}, the maximum NO conversion was up to 94 % at 230 °C, and when the GHSV was 9300 mL h^{-1} g^{-1}, the maximum conversion was approximately 92 % at 230 °C.

These results demonstrated that the GHSV was a crucial parameter for the H_2-SCR reaction and the space velocity determined the residence time of the gas in the catalyst. As GHSV increased, the residence time of feed gas decreased. The $NiCo_{1.95}Pd_{0.05}O_4$ catalyst showed high NO conversion with the increasing GHSV, due to the Pd addition, which enhanced the redox properties of the active catalyst component. And this was consistent with H_2-TPR. Although the increase of GHSV resulted in the decrease of the reaction gas residence time in the catalyst, the activity of the active component was enhanced in the Pd-doped catalyst, resulting in more reduction reaction sites for NO and only a slight decrease of NO conversion. Therefore, the Pd-doped $NiCo_{1.95}Pd_{0.05}O_4$ catalyst showed better catalytic performance than the $NiCo_2O_4$ catalyst at different GHSVs (from 4800 to 9300 mL h^{-1} g^{-1}).

The variation trend of NO conversion over the sample catalysts was roughly similar as the increase of reaction temperature at different NO/H_2 ratios, the NO conversion firstly increased then decreased over the $NiCo_{1.95}Pd_{0.05}O_4$ catalyst with the increasing reaction temperature, but the removal of NO over the $NiCo_2O_4$ catalyst increased as the temperature increased. As shown in Fig. 6c, the NO conversion over the $NiCo_2O_4$ catalyst decreased as the NO and H_2 feed concentration ratio increased within a temperature range of 170–350 °C in the presence of 2 % O_2. When the NO/H_2 ratio was 1:10, the maximum NO conversion was 41 %. When the NO/H_2 ratio was changed to 1:5 and 1:1, the NO conversion rate was 34 % and 31 %, respectively, exhibiting that higher H_2 concentration that resulted in higher NO conversion. Nevertheless, compared with the $NiCo_2O_4$ catalyst, the $NiCo_{1.95}Pd_{0.05}O_4$ catalyst showed higher catalytic activity at different NO and H_2 ratios, which is shown in Fig. 6d. When the NO/H_2 ratio was 1:10, the maximum NO conversion was

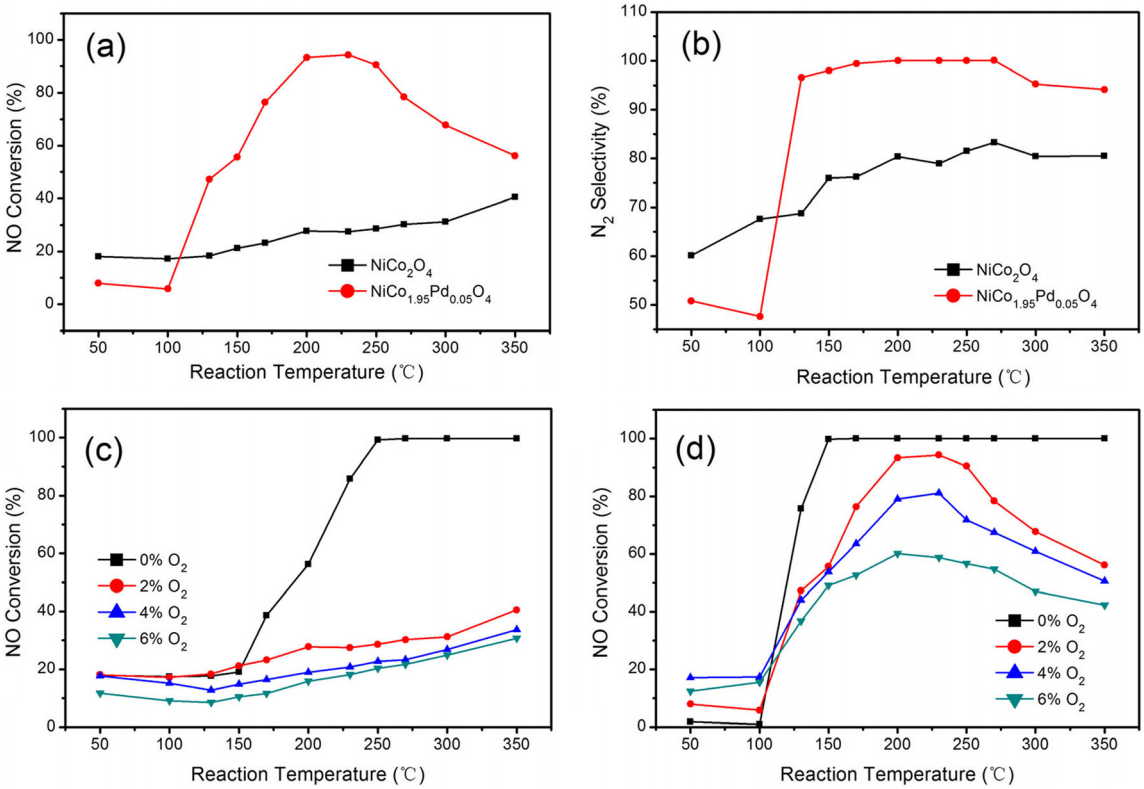

Fig. 5 **a** The effect of the reaction temperature on NO conversion for H_2-SCR over the $NiCo_2O_4$ and $NiCo_{1.95}Pd_{0.05}O_4$ catalysts in the presence of 2 % O_2. **b** N_2 selectivity over the $NiCo_2O_4$ and $NiCo_{1.95}Pd_{0.05}O_4$ catalysts in the presence of 2 % O_2. **c**, **d** The effect of oxygen concentration (0~6 %) on NO conversion for H_2-SCR over the $NiCo_2O_4$ and $NiCo_{1.95}Pd_{0.05}O_4$ catalysts. Reaction condition: [NO] = 1070 ppm; [H_2] = 10,700 ppm; [O_2] = 0 %, 2 % (**a**, **b**), 4 %, and 6 %; [N_2] = balance; catalyst mass = 1 g; GHSV = 4800 mL g^{-1} h^{-1}; and T = 50–350 °C. **c** $NiCo_2O_4$. **d** $NiCo_{1.95}Pd_{0.05}O_4$

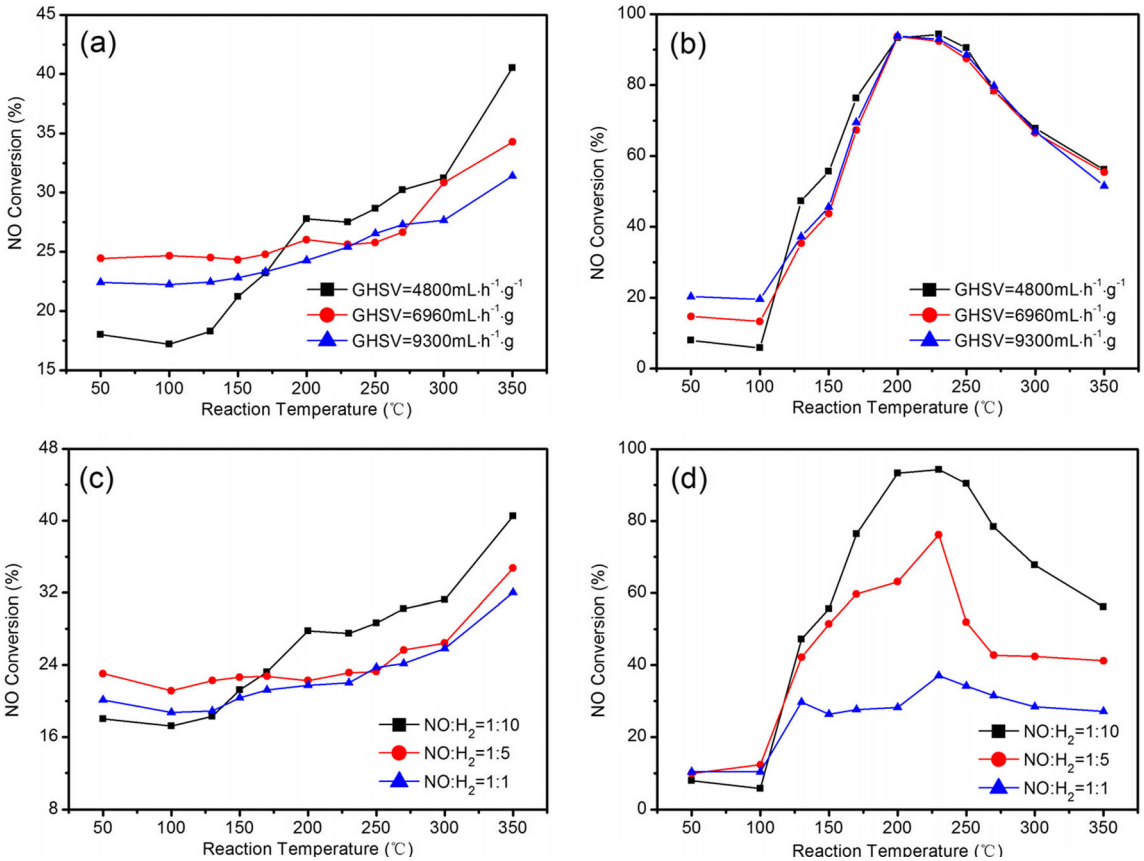

Fig. 6 Effect of gas hourly space velocity and NO/H_2 ratios on NO conversion for H_2-SCR over the $NiCo_{1.95}Pd_{0.05}O_4$ and $NiCo_2O_4$ catalysts. Reaction condition: [H_2] = 10,700 ppm (when examined gas hourly space velocity), [NO] = 1070 ppm, [O_2] = 2 %, [N2] = balance, catalyst mass = 1 g, GHSV = 4800 mL g^{-1} h^{-1} (when NO/H_2 ratios were examined), and T = 50–350 °C. **a** $NiCo_2O_4$. **b** $NiCo_{1.95}Pd_{0.05}O_4$. **c** $NiCo_2O_4$. **d** $NiCo_{1.95}Pd_{0.05}O_4$

more than 95 % at a reaction temperature of 230 °C. Actually, the economic factors must be considered. Industrially, the lower NO/H_2 ratio was used to obtain a relatively high NO conversion. When the NO/H_2 ratio was changed to 1:5 and 1:1, the NO conversion rate was 76 % and 37 %, respectively. Therefore, the doped Pd largely improved the catalytic activity and $NiCo_{1.95}Pd_{0.05}O_4$ exhibited higher catalytic performance than $NiCo_2O_4$ in the common reaction condition.

Effect of the presence of H_2O and SO_2

H_2O and SO_2 were usually contained in the industrial flue gases, which could cause a deactivation on SCR catalysts, and the general content of water was 2~10 %. At the same time, the SCR catalysts are sensitive to sulfur poisoning since sulfur compounds could deposit on the active sites of catalysts and deactivate them irreversibly (Chang et al. 2013; Lee et al. 2013; Yin et al. 2015). Therefore, it was important to investigate the effect of H_2O and SO_2 on NO conversion over selected catalysts.

The effect of H_2O and SO_2 on the selective catalytic reduction of nitric oxide with hydrogen over the $NiCo_2O_4$ and $NiCo_{1.95}Pd_{0.05}O_4$ catalyst was demonstrated in Fig. 7. As shown in Fig. 7a, when 2 %, 5 %, and 8 % H_2O was introduced to feed gas, the NO conversion of $NiCo_2O_4$ decreased rapidly from 36.8 %, 36.5 %, and 36.3 % to 33.2 %, 32.5 %, and 31.8 %, respectively, and then the NO conversion recovered slowly to 34.2 %, 33.4 %, and 32.6 % after the removal of H_2O, respectively. Compared with the initial value, the decrement of NO conversion was 7.07 %, 8.49 %, and 12.95 %, respectively. It could be seen that the conversion decreased more as the content of H_2O increased, which was due to the water-irreversible dissociative adsorption on the active sites of the catalyst (Burch and Coleman 1999; Leicht et al. 2012). And the NO conversion recovered a little, which was due to the reversible competitive adsorption by water. Hence, the influence of water on the catalyst was both reversible and irreversible.

However, the behavior of H_2O poisoning of the $NiCo_{1.95}Pd_{0.05}O_4$ catalyst was quite different. As shown in Fig. 7b, after 2 %, 5 %, and 8 % H_2O was introduced into the inlet gas, the NO conversion showed a slight decrease approximately from 87.2 % to 86.5 %, 84.5 %, and 80.5 %, respectively, which probably was due to the H_2O competitive adsorption with NO as well as with H_2. The water on the

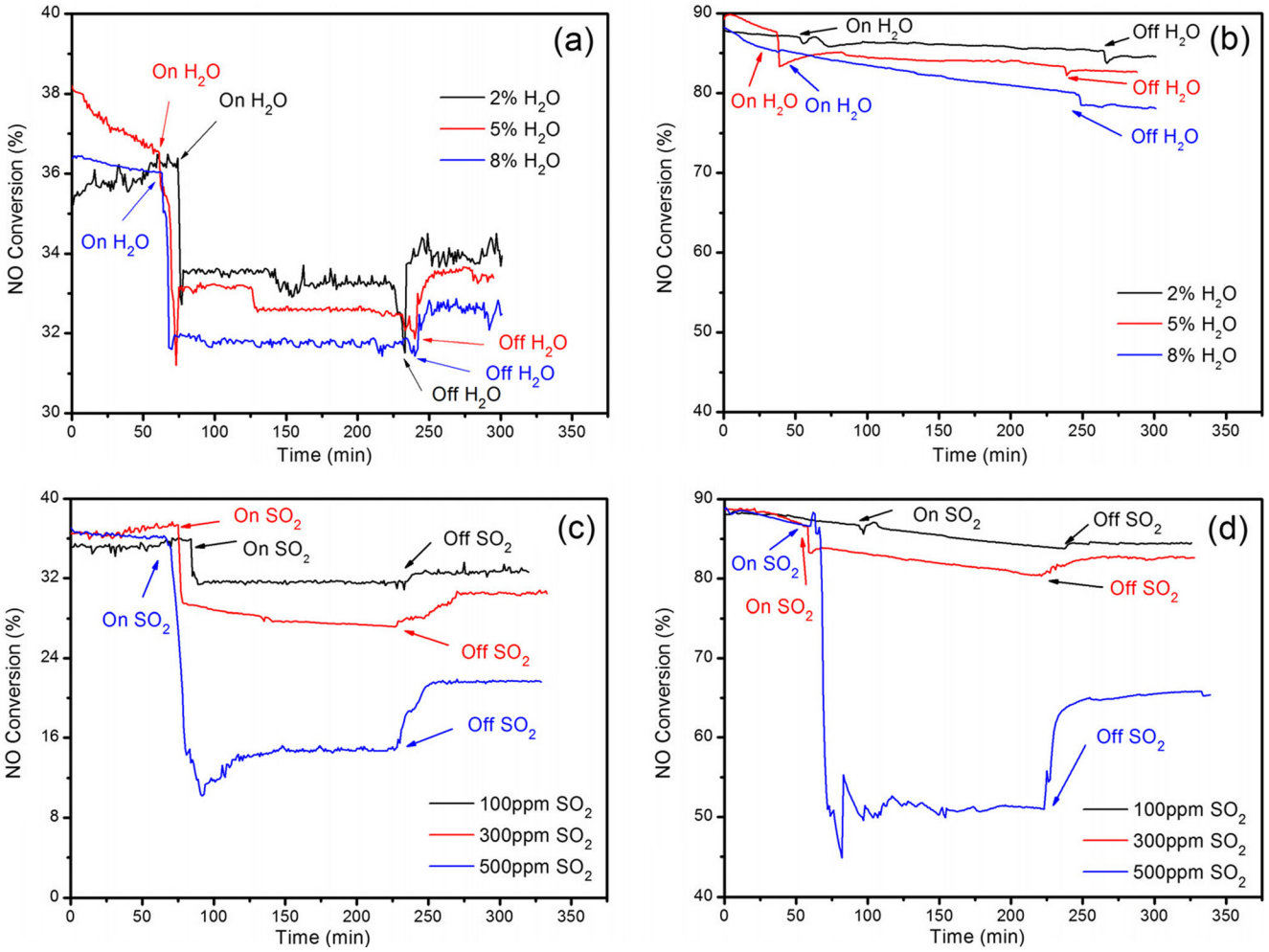

Fig. 7 Effect of H_2O ([H_2O] = 2 %, 5 %, and 8 %) and SO_2 ([SO_2] = 100, 300, and 500 ppm) on NO conversion for H_2-SCR over the $NiCo_2O_4$ and $NiCo_{1.95}Pd_{0.05}O_4$ catalysts. Reaction condition: [NO] = 930 ppm (950 ppm, when SO_2 was added), [H_2] = 9300 ppm (9500 ppm, when SO_2 was added), [O_2] = 2 %, [N2] = balance, catalyst mass = 1 g, GHSV = 9300 mL g^{-1} h^{-1}, and flow rate = 155 mL/min. **a** $NiCo_2O_4$, T = 350 °C, when H_2O was added. **b** $NiCo_{1.95}Pd_{0.05}O_4$, T = 230 °C, when H_2O was added. **c** $NiCo_2O_4$, T = 350 °C, when SO_2 was added. **d** $NiCo_{1.95}Pd_{0.05}O_4$, T = 230 °C, when SO_2 was added

catalyst could form the additional surface hydroxyls because of the dissociative adsorption of water (Kijlstra et al. 1996), and the surface hydroxyls would neutralize the acid sites, resulting in the reduction of SCR activity. For the Pd-doped catalyst, the surface acidity was enhanced. The multi-acid neutralized the hydroxyls and decreased the water poisoning on active sites of the catalyst. Therefore, the $NiCo_{1.95}Pd_{0.05}O_4$ catalyst has a better H_2O tolerance than $NiCo_2O_4$. Furthermore, the influence of surface hydroxyls neutralizing the acid sites was irreversible; when the H_2O was off, the acidity of acid sites could not recover, and hence, the NO conversion over the $NiCo_{1.95}Pd_{0.05}O_4$ catalyst could not restore to the original level, which was consistent with Fig. 7b.

Moreover, the SO_2 tolerance and regenerability of $NiCo_2O_4$ and $NiCo_{1.95}Pd_{0.05}O_4$ catalysts were also examined. As shown in Fig. 7c, when the 100 ppm SO_2 was added to the reactant gas, the NO conversion of $NiCo_2O_4$ at 350 °C decreased rapidly from 35.8 % to 31.6 % in 150 min and only recovered to 32.6 % after the removal of SO_2, manifesting the inhibition effect of SO_2 on the SCR activity over $NiCo_2O_4$ (Chang et al. 2013; Yin et al. 2015). When the SO_2 increased to 300 and 500 ppm, the NO conversion decreased rapidly to lower than 27.5 % and 14.5 % and only recovered to 30.6 % and 21.6 % after the removal of SO_2, respectively. The decrease of NO conversion was mainly due to the blocking of the active sites by the formation of metal sulfates and/or sulfites (Li et al. 2011). The sulfated species formed on the catalytic center inhibited the SCR activity, which resulted in the decrease of NO conversion. After the supply of SO_2 was cut off, the NO conversion recovered slowly in a certain amount, which was mainly due to the regeneration of the part of sulfated catalysts by the hydrogen (Wang et al. 2015a).

The SO_2 poisoning behavior to the $NiCo_{1.95}Pd_{0.05}O_4$ catalyst at 230 °C was quite similar. As shown in Fig. 7d, after 100, 300, and 500 ppm SO_2 was introduced to the inlet gas, the NO conversion of $NiCo_{1.95}Pd_{0.05}O_4$ decreased steadily

from 88.1 % to 83.8 %, 80.5 %, and 51.6 % in 130 min, respectively. The decrement of NO conversion was 4.88 %, 8.63 %, and 41.43 % compared to the initial value; however, the decrement value of $NiCo_2O_4$ was 11.73 %, 23.18 %, and 59.50 %, respectively. This was attributed to the improvement of catalytic activity by enhanced surface acidities and redox properties, which was consistent with NH_3-TPD and H_2-TPR. After 100, 300, and 500 ppm SO_2 was off, the NO conversion of $NiCo_{1.95}Pd_{0.05}O_4$ could efficiently recover to 84.4 %, 82.8 %, and 65.5 %, respectively, indicating that the deactivation was partially reversible.

These results demonstrated that the $NiCo_{1.95}Pd_{0.05}O_4$ catalyst possesses better SO_2 tolerance than $NiCo_2O_4$ catalyst does.

Conclusions

In this study, the $NiCo_2O_4$ and $NiCo_{1.95}Pd_{0.05}O_4$ catalysts were investigated for NO selective reduction by hydrogen in the presence of O_2. The results showed that the $NiCo_2O_4$ catalyst had a certain effect for NO removal, while the Pd-containing $NiCo_{1.95}Pd_{0.05}O_4$ catalyst exhibited better SCR activity with the maximum NO conversion of 94.65 % at 230 °C and the N_2 selectivity of 100 %. Moreover, the prepared $NiCo_{1.95}Pd_{0.05}O_4$ exhibited higher H_2O and SO_2 tolerance than $NiCo_2O_4$.

Acknowledgments This research is based on the work supported by the National Natural Science Foundation of China (21277045). Thanks to Zhenhua Zhou and Baosheng Tu for providing solutions to the experimental process and writing assistance.

References

Auxilia FM, Ishihara S, Mandal S, Tanabe T, Saravanan G, Ramesh GV, Umezawa N, Hara T, Xu Y, Hishita S (2014) Low-temperature remediation of NO catalyzed by interleaved CuO nanoplates. Adv Mater 26:4481–4485

Babu GA, Ravi G, Hayakawa Y (2014) Surfactant assisted growth and optical studies of $NiCo_2O_4$ nanostructures through microwave heating method. Int J Sci Eng Appl 1:17–20

Burch R, Coleman MD (1999) An investigation of the $NO/H_2/O_2$ reaction on noble-metal catalysts at low temperatures under lean-burn conditions. Appl Catal B Environ 23:115–121

Chang H, Li J, Yuan J, Chen L, Dai Y, Arandiyan H, Xu J, Hao J (2013) Ge, Mn-doped CeO_2–WO_3 catalysts for NH_3–SCR of NOx: effects of SO_2 and H_2 regeneration. Catal Today 201:139–144

Chen X, Zhang JF, Huang Y, Tong ZQ, Huang M (2009) Catalytic reduction of nitric oxide with carbon monoxide on copper-cobalt oxides supported on nano-titanium dioxide. J Environ Sci 21: 1296–1301

Chi B, Lin H, Li J, Wang N, Yang J (2006) Comparison of three preparation methods of $NiCo_2O_4$ electrodes. Int J Hydrog Energy 31:1210–1214

Chiarello GL, Ferri D, Grunwaldt JD, Forni L, Baiker A (2007) Flame-synthesized $LaCoO_3$-supported Pd: 2. Catalytic behavior in the reduction of NO by H_2 under lean conditions. J Catal 252:137–147

Chiu CH, Hsi HC, Lin HP (2015) Multipollutant control of $Hg/SO_2/NO$ from coal-combustion flue gases using transition metal oxide-impregnated SCR catalysts. Catal Today 245:2–9

Costa CN, Efstathiou AM (2007a) Low-temperature H_2-SCR of NO on a novel $Pt/MgO\text{-}CeO_2$ catalyst. Appl Catal B Environ 72:240–252

Costa CN, Efstathiou AM (2007b) Mechanistic aspects of the H_2-SCR of NO on a novel $Pt/MgO\text{-}CeO_2$ catalyst. J Phys Chem C 111:3010–3020

Du Y, Huang W, Hua Z, Wang Y, Cui X, Wu M, Shu Z, Zhang L, Wang J, Chen H (2014) A facile ultrasonic process for the preparation of Co_3O_4 nanoflowers for room-temperature removal of low-concentration NOx. Catal Commun 57:73–77

Fan J, Huang W (2011) Preparation of Cu-Zn-Al bifunctional catalyst by sol-gel method with the assistance of PEG and its catalytic performance. Chin J Catal 32:139–143

Fino D, Russo N, Saracco G, Specchia V (2008) Removal of NOx and diesel soot over catalytic traps based on spinel-type oxides. Powder Technol 180:74–78

Fritz A, Pitchon V (1997) The current state of research on automotive lean NOx catalysis. Appl Catal B Environ 13:1–25

Gaspar AB, Dieguez LC (2000) Dispersion stability and methylcyclopentane hydrogenolysis in Pd/Al 2 O 3 catalysts. Appl Catal A Gen 201:241–251

Giraudon JM, Elhachimi A, Wyrwalski F, Siffert S, Aboukaïs A, Lamonier JF, Leclercq G (2007) Studies of the activation process over Pd perovskite-type oxides used for catalytic oxidation of toluene. Appl Catal B Environ 75:157–166

Gou Y, Liang X, Chen B (2013) Porous Ni–Co bimetal oxides nanosheets and catalytic properties for CO oxidation. J Alloys Compd 574:181–187

Grossale A, Nova I, Tronconi E (2008) Study of a Fe–zeolite-based system as NH_3-SCR catalyst for diesel exhaust after treatment. Catal Today 136:18–27

Hu L, Peng Q, Li Y (2011) Low-temperature CH_4 catalytic combustion over Pd catalyst supported on Co_3O_4 nanocrystals with well-defined crystal planes. ChemCatChem 3:868–874

Huilin L, Guangbo Z, Rushan B, Yongjin C, Gidaspow D (2000) A coal combustion model for circulating fluidized bed boilers. Fuel 79:165–172

Iliev MN, Silwal P, Loukya B, Datta R, Kim DH, Todorov ND, Pachauri N, Gupta A (2013) Raman studies of cation distribution and thermal stability of epitaxial spinel $NiCo_2O_4$ films. J Appl Phys 114: 033514–033514-5

Imran M, Kim DH, Al-Masry WA, Mahmood A, Hassan A, Haider S, Ramay SM (2013) Manganese-, cobalt-, and zinc-based mixed-oxide spinels as novel catalysts for the chemical recycling of poly(ethylene terephthalate) via glycolysis. Polym Degrad Stab 98:904–915

Jauhar S, Goyal A, Lakshmi N, Chandra K, Singhal S (2013) Doping effect of Cr^{3+} ions on the structural, magnetic and electrical properties of Co–Cd ferrites: a study on the redistribution of cations in $CoCd_{0.4}Cr_xFe_{1.6-x}O_4$ ($0.1 \le x \le 0.6$) ferrites. Mater Chem Phys 139:836–843

Jun Yub L, Bum KS, Sung Chang H (2003) Characterization and reactivity of natural manganese ore catalysts in the selective catalytic oxidation of ammonia to nitrogen. Chemosphere 50:1115–1122

Kavas H, Baykal A, Toprak MS, Köseoğlu Y, Sertkol M, Aktaş B (2009) Cation distribution and magnetic properties of Zn doped NiFe2O4 nanoparticles synthesized by PEG-assisted hydrothermal route. J Alloys Compd 479:49–55

Kijlstra WS, Daamen JCML, Graaf JMVD, Linden BVD, Poels EK, Bliek A (1996) Inhibiting and deactivating effects of water on the selective catalytic reduction of nitric oxide with ammonia over $MnOx/Al_2O_3$. Appl Catal B Environ 7:337–357

Kim SS, Hong SC (2010) Relationship between the surface characteristics of Pt catalyst and catalytic performance on the H_2-SCR. J Ind Eng Chem 16:992–996

Kim JG, Pugmire DL, Battaglia D, Langell MA (2000) Analysis of the $NiCo_2O_4$ spinel surface with Auger and X-ray photoelectron spectroscopy. Appl Surf Sci 165:70–84

Koebel M, Elsener M, Madia G (2001) Reaction pathways in the selective catalytic reduction process with NO and NO_2 at low temperatures. Ind Eng Chem Res 40:52–59

Lee KJ, Maqbool MS, Kumar PA, Song KH, Ha HP (2013) Enhanced activity of ceria loaded Sb-V_2O_5/TiO_2 catalysts for NO reduction with ammonia. Catal Lett 143:988–995

Leicht M, Schott FJP, Bruns M, Kureti S (2012) NOx reduction by H_2 on WOx/ZrO_2-supported Pd catalysts under lean conditions. Appl Catal B Environ 117–118:275–282

Li L, Zhang F, Guan N, Schreier E, Richter M (2008) NO selective reduction by hydrogen on potassium titanate supported palladium catalyst. Catal Commun 9:1827–1832

Li JH, Wang CC, Huang CJ, Sun YF, Weng WZ, Wan HL (2010a) Mesoporous nickel oxides as effective catalysts for oxidative dehydrogenation of propane to propene. Appl Catal A Gen 382:99–105

Li L, Wu P, Yu Q, Wu G, Guan N (2010b) Low temperature H_2-SCR over platinum catalysts supported on Ti-containing MCM-41. Appl Catal B Environ 94:254–262

Li J, Chang H, Ma L, Hao J, Yang RT (2011) Low-temperature selective catalytic reduction of NOx with NH_3 over metal oxide and zeolite catalysts—a review. Catal Today 175:147–156

Li J, Wu G, Guan N, Li L (2012) NO selective reduction by hydrogen over bimetallic Pd–Ir/TiO_2 catalyst. Catal Commun 24:38–43

Li D, Gong Y, Zhang Y, Luo C, Li W, Fu Q, Pan C (2015) Facile synthesis of carbon nanosphere/$NiCo_2O_4$ core-shell sub-microspheres for high performance supercapacitor. Sci Rep 5

Lim TH, Cho SJ, Yang HS, Engelhard MH, Kim DH (2015) Effect of Co/Ni ratios in cobalt nickel mixed oxide catalysts on methane combustion. Appl Catal A Gen 505:62–69

Ling F, Anthony OC, Xiong Q, Luo M, Pan X, Jia L, Huang J, Sun D, Li Q (2015): PdO/$LaCoO_3$ heterojunction photocatalysts for highly hydrogen production from formaldehyde aqueous solution under visible light. Int J Hydrogen Energ

Liu ZQ, Xiao K, Xu QZ, Li N, Su YZ, Wang HJ, Chen S (2013) Fabrication of hierarchical flower-like super-structures consisting of porous $NiCo_2O_4$ nanosheets and their electrochemical and magnetic properties. RSC Adv 3:4372–4380

Lou XW, Deng D, Lee JY, Archer LA (2008) Thermal formation of mesoporous single-crystal Co_3O_4 nano-needles and their lithium storage properties. J Mater Chem 18:4397–4401

Machida M, Ikeda S, Kurogi D, Kijima T (2001) Low temperature catalytic NOx–H_2 reactions over Pt/TiO_2-ZrO_2 in an excess oxygen. Appl Catal B Environ 35:107–116

Moni P, Kriangsak K, Sangaraju S (2014) Hierarchical nanostructured $NiCo_2O_4$ as an efficient bifunctional non-precious metal catalyst for rechargeable zinc-air batteries. Nanoscale 6:3173–3181

Olympiou GG, Efstathiou AM (2011) Industrial NOx control via H_2-SCR on a novel supported-Pt nanocatalyst. Chem Eng J 170:424–432

Qi G, Yang RT, Rinaldi FC (2006) Selective catalytic reduction of nitric oxide with hydrogen over Pd-based catalysts. J Catal 237:381–392

Qing YU, Kong F, Landong LI, Guangjun WU (2010) Fast catalytic reduction of NOx by H_2 over Pd-based catalysts. Chin J Catal 31:261–263

Rodríguez GCM, Saruhan B (2010) Effect of Fe/Co ratio on the phase composition of Pd-integrated perovskites and its H_2-SCR of NOx performance. Appl Catal B Environ 93:304–313

Rui D, Li Q, Jia M, Wang H (2013) Facile and large-scale chemical synthesis of highly porous secondary submicron/micron-sized $NiCo_2O_4$ materials for high-performance aqueous hybrid AC-$NiCo_2O_4$ electrochemical capacitors. Electrochim Acta 107:494–502

Schott FJP, Balle P, Adler J, Kureti S (2009) Reduction of NOx by H_2 on Pt/WO_3/ZrO_2 catalysts in oxygen-rich exhaust. Appl Catal B Environ 87:18–29

Wang Z, Dong Y, Chunyuan, Sun S (2009) Influence of temperature change on conversion characteristics of NOx in the reburning zone. Intl Conf En Env Technol 707–710

Wang X, Jiang L, Wang J, Wang R (2015a) Ag/bauxite catalysts: improved low-temperature activity and SO_2 tolerance for H_2-promoted NH_3-SCR of NOx. Appl Catal B Environ 165:700–705

Wang X, Wen W, Mi J, Li X, Wang R (2015b) The ordered mesoporous transition metal oxides for selective catalytic reduction of NOx at low temperature. Appl Catal B Environ 176–177:454–463

Wei Y, Runduo Z, Biaohua C, Daniel D, Sébastien R (2012) New aspects on the mechanism of C_3H_6 selective catalytic reduction of NO in the presence of O_2 over $LaFe_{1-x}(Cu, Pd)_xO_{3-\delta}$ perovskites. Environ Sci Technol 46:11280–11288

Weirong GU, Zhou M, Wei MA, Wang Y (2012) Research progress on selective catalytic reduction de-NOx catalysts. Chem Ind Eng Progress 31:1493–1500

Xiaoling M, Bingsen Z, Yong L, Lide Y, Xuejiao W, Dang Sheng S, Wenjie S (2012) Rod-shaped Fe_2O_3 as an efficient catalyst for the selective reduction of nitrogen oxide by ammonia. Angew Chem 51:2989–2993

Xu J, He L, Xu W, Tang H, Liu H, Han T, Zhang C, Zhang Y (2014) Facile synthesis of porous NiCo2O4 microflowers as high-performance anode materials for advanced lithium-ion batteries. Electrochim Acta 145:185–192

Xu C, Sun W, Cao L, Yang J (2015) Selective catalytic reduction of nitric oxide by hydrogen over $NiFe_{2-x}Pd_xO_4$ catalysts at low temperature. Chem Eng J 283

Yang JI, Jung H (2009) The effect of temperature on NOx reduction by H_2 in the presence of excess oxygen on a Pt/Al_2O_3 monolithic catalyst. Chem Eng J 146:11–15

Yang S, Wang X, Chu W, Song Z, Zhao S (2011) An investigation of the surface intermediates of H_2-SCR of NOx over Pt/H-FER. Appl Catal B Environ 3:380–385

Yin C, Wang L, Rivillon S, Shih AJ, Yang RT (2015) SCR of nitric oxide by hydrogen over Pd and Ir based catalysts with different supports. Catal Lett 145:1491–1499

Yu Z, Li H, Zhang X, Liu N, Tan W, Zhang X, Zhang L (2016) Facile synthesis of $NiCo_2O_4$@polyaniline core-shell nanocomposite for sensitive determination of glucose. Biosens Bioelectron 75:161–165

Yuan L, Zheng X, Duan K, Hu H, Wang J, Woo SI, Liu Z (2013) The effect of preparation conditions of Pt/Al_2O_3 on its catalytic performance for the H_2-SCR in the presence of oxygen. Fron Env Sci Eng 7:457–463